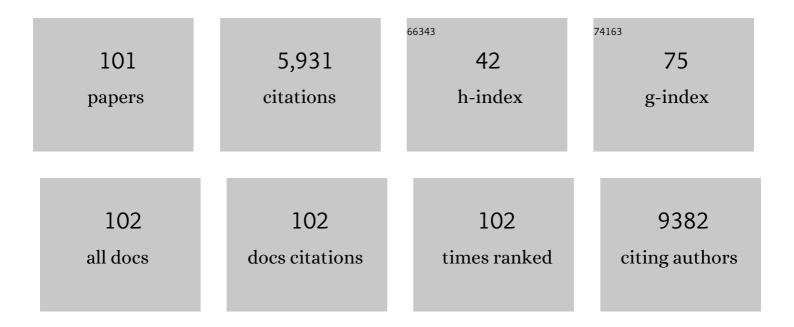
## Chun Li

## List of Publications by Year in descending order

Source: https://exaly.com/author-pdf/6315138/publications.pdf Version: 2024-02-01



СыныТт

#	Article	IF	CITATIONS
1	Bistable Silver Electrodepositionâ€Based Electrochromic Device with Reversible Threeâ€State Optical Transformation By Using WO <sub>3</sub> Nanoislands Modified ITO Electrode. Advanced Materials Interfaces, 2022, 9, .	3.7	5
2	Room-temperature Near-infrared Excitonic Lasing from Mechanically Exfoliated InSe Microflake. ACS Nano, 2022, 16, 1477-1485.	14.6	11
3	Ultrafast Antisolvent Growth of Single-Crystalline CsPbCl <sub>3</sub> Microcavity for Low-Threshold Room Temperature Blue Lasing. ACS Applied Materials & Interfaces, 2022, 14, 21356-21362.	8.0	6
4	2D WS <sub>2</sub> : From Vapor Phase Synthesis to Device Applications. Advanced Electronic Materials, 2021, 7, 2000688.	5.1	63
5	Strong exciton-photon interaction and lasing of two-dimensional transition metal dichalcogenide semiconductors. Nano Research, 2021, 14, 1937-1954.	10.4	36
6	Gate-bias instability of few-layer WSe <sub>2</sub> field effect transistors. RSC Advances, 2021, 11, 6818-6824.	3.6	6
7	High Optical Gain of Solutionâ€Processed Mixedâ€Cation CsPbBr <sub>3</sub> Thin Films towards Enhanced Amplified Spontaneous Emission. Advanced Functional Materials, 2021, 31, 2102210.	14.9	35
8	Millimeter-scale growth of highly ordered CsPbBr <sub>3</sub> single-crystalline microplatelets on SiO <sub>2</sub> /Si substrate by chemical vapor deposition. Journal Physics D: Applied Physics, 2021, 54, 334004.	2.8	4
9	Enhanced responsivity of a graphene/Si-based heterostructure broadband photodetector by introducing a WS <sub>2</sub> interfacial layer. Journal of Materials Chemistry C, 2021, 9, 3846-3853.	5.5	28
10	Enhanced epitaxial growth of two-dimensional monolayer WS2 film with large single domains. Applied Materials Today, 2021, 25, 101234.	4.3	4
11	Enhanced Optical Absorption and Slowed Light of Reduced-Dimensional CsPbBr <sub>3</sub> Nanowire Crystal by Exciton–Polariton. Nano Letters, 2020, 20, 1023-1032.	9.1	55
12	Graphoepitaxy of Large Scale, Highly Ordered CsPbBr 3 Nanowire Array on Muscovite Mica (001) Driven by Surface Reconstructed Grooves. Advanced Optical Materials, 2020, 8, 2000743.	7.3	15
13	Plasmonic Nanolasers in On-Chip Light Sources: Prospects and Challenges. ACS Nano, 2020, 14, 14375-14390.	14.6	52
14	A Strategy for High-Performance Photodetector based on Graphene-Si heterostructure. E3S Web of Conferences, 2020, 213, 02014.	0.5	0
15	Electrochromic and energy storage bifunctional Gd-doped WO <sub>3</sub> /Ag/WO <sub>3</sub> films. Journal of Materials Chemistry A, 2020, 8, 10973-10982.	10.3	22
16	2D materials beyond graphene toward Si integrated infrared optoelectronic devices. Nanoscale, 2020, 12, 11784-11807.	5.6	59
17	Ag nanorods assembled with ZnO nanowalls for near-linear high-response UV photodetectors. Journal of Alloys and Compounds, 2020, 830, 154652.	5.5	25
18	Evaluation and Dynamic Mechanism of Ecological Space in a Densely Urbanized Region During a Rapidly Growing Period—A Case Study of the Wu-E-Huang-Huang Metropolitan Interlocking Region. Sustainability, 2020, 12, 73.	3.2	3

#	Article	IF	CITATIONS
19	Sputter deposition of Ag-induced WO3 nanoisland films with enhanced electrochromic properties. Journal of Alloys and Compounds, 2020, 829, 154431.	5.5	13
20	Mediator–Antisolvent Strategy to Stabilize All-Inorganic CsPbI <sub>3</sub> for Perovskite Solar Cells with Efficiency Exceeding 16%. ACS Energy Letters, 2020, 5, 1619-1627.	17.4	46
21	Graphene/WS <sub>2</sub> heterostructure saturable absorbers for ultrashort pulse generation in L-band passively mode-locked fiber lasers. Optics Express, 2020, 28, 11514.	3.4	36
22	Semiconductor nanowire plasmonic lasers. Nanophotonics, 2019, 8, 2091-2110.	6.0	40
23	High Performance Van der Waals Graphene–WS <sub>2</sub> –Si Heterostructure Photodetector. Advanced Materials Interfaces, 2019, 6, 1901304.	3.7	41
24	Surfaceâ€Plasmonâ€Assisted Metal Halide Perovskite Small Lasers. Advanced Optical Materials, 2019, 7, 1900279.	7.3	35
25	Photoluminescence properties of ultrathin CsPbCl3 nanowires on mica substrate. Journal of Semiconductors, 2019, 40, 052201.	3.7	16
26	Temperature-dependent photoluminescence and lasing properties of CsPbBr3 nanowires. Applied Physics Letters, 2019, 114, .	3.3	59
27	Synthesis of large-area uniform MoS <sub>2</sub> films by substrate-moving atmospheric pressure chemical vapor deposition: from monolayer to multilayer. 2D Materials, 2019, 6, 025030.	4.4	33
28	Lasing from reduced dimensional perovskite microplatelets: Fabry-Pérot or whispering-gallery-mode?. Journal of Chemical Physics, 2019, 151, 211101.	3.0	12
29	Passively Q-switched and mode-locked Tm-Ho co-doped fiber laser using a WS2 saturable absorber fabricated by chemical vapor deposition. Optics and Laser Technology, 2019, 111, 571-574.	4.6	52
30	Effect of Gd-doping on electrochromic properties of sputter deposited WO3 films. Journal of Alloys and Compounds, 2018, 739, 623-631.	5.5	37
31	Wafer-scale synthesis of monolayer WS2 for high-performance flexible photodetectors by enhanced chemical vapor deposition. Nano Research, 2018, 11, 3371-3384.	10.4	190
32	Surface Plasmon Enhanced Strong Exciton–Photon Coupling in Hybrid Inorganic–Organic Perovskite Nanowires. Nano Letters, 2018, 18, 3335-3343.	9.1	133
33	Solvothermal synthesis of cesium lead halide perovskite nanowires with ultra-high aspect ratios for high-performance photodetectors. Nanoscale, 2018, 10, 21451-21458.	5.6	61
34	Facile large-area autofocusing Raman mapping system for 2D material characterization. Optics Express, 2018, 26, 9071.	3.4	10
35	Novel Series of Quasi-2D Ruddlesden–Popper Perovskites Based on Short-Chained Spacer Cation for Enhanced Photodetection. ACS Applied Materials & Interfaces, 2018, 10, 19019-19026.	8.0	75
36	Highly responsive and broadband photodetectors based on WS <sub>2</sub> –graphene van der Waals epitaxial heterostructures. Journal of Materials Chemistry C, 2017, 5, 1494-1500.	5.5	103

#	Article	IF	CITATIONS
37	Transparent, flexible, and stretchable WS <sub>2</sub> based humidity sensors for electronic skin. Nanoscale, 2017, 9, 6246-6253.	5.6	288
38	ZnO–WS <sub>2</sub> heterostructures for enhanced ultra-violet photodetectors. RSC Advances, 2016, 6, 67520-67524.	3.6	54
39	CdS nanowire-modified 3D graphene foam for high-performance photo-electrochemical anode. Journal of Alloys and Compounds, 2016, 688, 37-43.	5.5	8
40	Zener Tunneling and Photoresponse of a WS <sub>2</sub> /Si van der Waals Heterojunction. ACS Applied Materials & Interfaces, 2016, 8, 18375-18382.	8.0	101
41	Passively Q-switched mid-infrared fluoride fiber laser around 3 <i>µ</i> m using a tungsten disulfide (WS <sub>2</sub> ) saturable absorber. Laser Physics Letters, 2016, 13, 105108.	1.4	75
42	Reactive Sputter Deposition of WO <sub>3</sub> /Ag/WO <sub>3</sub> Film for Indium Tin Oxide (ITO)-Free Electrochromic Devices. ACS Applied Materials & Interfaces, 2016, 8, 3861-3867.	8.0	87
43	Femtosecond Er-doped fiber laser using a graphene/MoS2 heterostructure saturable absorber. , 2016, ,		1
44	Passive harmonic mode-locking of Er-doped fiber laser using CVD-grown few-layer MoS <sub> <b>2</b> </sub> as a saturable absorber. Chinese Physics B, 2015, 24, 084206.	1.4	11
45	Field emission properties of ZnO nanorod arrays by few seed layers assisted growth. Applied Surface Science, 2015, 331, 497-503.	6.1	24
46	Large-area synthesis of monolayer WS <sub>2</sub> and its ambient-sensitive photo-detecting performance. Nanoscale, 2015, 7, 5974-5980.	5.6	211
47	Synthesis of single-crystalline GeS nanoribbons for high sensitivity visible-light photodetectors. Journal of Materials Chemistry C, 2015, 3, 8074-8079.	5.5	111
48	Few-layer MoS_2 grown by chemical vapor deposition as a passive Q-switcher for tunable erbium-doped fiber lasers. Photonics Research, 2015, 3, A92.	7.0	48
49	Passively <inline-formula> <tex-math notation="LaTeX">\$Q\$ </tex-math></inline-formula> -Switched Erbium-Doped Fiber Laser Based on Few-Layer MoS <sub>2</sub> Saturable Absorber. IEEE Photonics Technology Letters, 2015, 27, 69-72.	2.5	106
50	Erbium-doped fiber laser mode-locked with a few-layer MoS2 saturable absorber. , 2014, , .		1
51	Ultrafast erbium-doped fiber laser mode-locked by a CVD-grown molybdenum disulfide (MoS_2) saturable absorber. Optics Express, 2014, 22, 17341.	3.4	281
52	Effect of thermal annealing on the performance of WO 3 –Ag–WO 3 transparent conductive film. Thin Solid Films, 2014, 571, 134-138.	1.8	24
53	Optical properties of (100) oriented ZnO:Gd films deposited by reactive radio frequency magnetron sputtering. Materials Letters, 2014, 132, 116-118.	2.6	12
54	Catalyst-Free Heteroepitaxial MOCVD Growth of InAs Nanowires on Si Substrates. Journal of Physical Chemistry C, 2014, 118, 1696-1705.	3.1	38

#	Article	IF	CITATIONS
55	Epitaxial Nanosheet–Nanowire Heterostructures. Nano Letters, 2013, 13, 948-953.	9.1	54
56	Substrate Mediation in Vapor Deposition Growth of Layered Chalcogenide Nanoplates: A Case Study of SnSe <sub>2</sub> . Journal of Physical Chemistry C, 2013, 117, 6469-6475.	3.1	86
57	Controlled Scalable Synthesis of Uniform, High-Quality Monolayer and Few-layer MoS2 Films. Scientific Reports, 2013, 3, 1866.	3.3	753
58	Tactile Feedback Display with Spatial and Temporal Resolutions. Scientific Reports, 2013, 3, 2521.	3.3	21
59	Improved thermal stability of antimonyâ€doped amorphous selenium film for Xâ€ray flatâ€panel detectors. Physica Status Solidi (A) Applications and Materials Science, 2013, 210, 580-584.	1.8	7
60	3D branched nanowire heterojunction photoelectrodes for high-efficiency solar water splitting and H2 generation. Nanoscale, 2012, 4, 1515.	5.6	167
61	Role of Boundary Layer Diffusion in Vapor Deposition Growth of Chalcogenide Nanosheets: The Case of GeS. ACS Nano, 2012, 6, 8868-8877.	14.6	137
62	Seed-Layer-Assisted Synthesis of Well-Aligned Zinc Oxide Nanorod Arrays for Field Emission Application. , 2012, , 491-511.		0
63	"Chemical Blowing―of Thinâ€Walled Bubbles: Highâ€Throughput Fabrication of Largeâ€Area, Few‣ayered and C <i><sub>x</sub></i> â€BN Nanosheets. Advanced Materials, 2011, 23, 4072-4076.	BN 21.0	217
64	Selfâ€condensing atom transfer radical polymerization of inimers of different reactivity ratios with styrene and the thermal properties of poly(2,6â€dimethylâ€1, 4â€phenylene oxide)/branched polystyrene blends. Journal of Applied Polymer Science, 2011, 121, 2957-2968.	2.6	2
65	Effect of Size-Dependent Thermal Instability on Synthesis of Zn2SiO4-SiO x Core–Shell Nanotube Arrays and Their Cathodoluminescence Properties. Nanoscale Research Letters, 2010, 5, 773-780.	5.7	19
66	Self-assembled ZnS nanowire arrays: synthesis, <i>in situ</i> Cu doping and field emission. Nanotechnology, 2010, 21, 375601.	2.6	27
67	Batch production of single-crystal diamond bridges and cantilevers for microelectromechanical systems. Journal of Micromechanics and Microengineering, 2010, 20, 085002.	2.6	36
68	Solution Synthesis of Large-Scale, High-Sensitivity ZnO/Si Hierarchical Nanoheterostructure Photodetectors. Journal of the American Chemical Society, 2010, 132, 15465-15467.	13.7	118
69	Synthesis of In <sub>2</sub> O <sub>3</sub> Nanowire-Decorated Ga <sub>2</sub> O <sub>3</sub> Nanobelt Heterostructures and Their Electrical and Field-Emission Properties. ACS Nano, 2010, 4, 2452-2458.	14.6	60
70	Current Imaging and Electromigration-Induced Splitting of GaN Nanowires As Revealed by Conductive Atomic Force Microscopy. ACS Nano, 2010, 4, 2422-2428.	14.6	18
71	Visible-blind deep-ultraviolet Schottky photodetector with a photocurrent gain based on individual Zn2GeO4 nanowire. Applied Physics Letters, 2010, 97, .	3.3	89
72	Synthesis of patterned carbon nanotube arrays for field emission using a two layer Sn/Ni catalyst in an ethanol flame. Diamond and Related Materials, 2009, 18, 1375-1380.	3.9	14

#	Article	IF	CITATIONS
73	Thickness-dependent bending modulus of hexagonal boron nitride nanosheets. Nanotechnology, 2009, 20, 385707.	2.6	134
74	Influence of substrate temperature on electrical and optical properties of p-type semitransparent conductive nickel oxide thin films deposited by radio frequency sputtering. Applied Surface Science, 2008, 254, 2401-2405.	6.1	139
75	Field emission enhancement of ZnO nanorod arrays with hafnium nitride coating. Surface and Coatings Technology, 2008, 202, 3480-3484.	4.8	42
76	Synthesis and photoluminescence, field emission properties of stalactite-like ZnS-ZnO composite nanostructures. Applied Physics A: Materials Science and Processing, 2008, 90, 759-763.	2.3	5
77	Oxygen-ion diffusion and electrical conduction of La2Mo2â^2x Fe x O9â^1^ systems. Frontiers of Materials Science in China, 2008, 2, 42-47.	0.5	2
78	Fabrication and electrical and photosensitive properties of silicon nanowire p–n homojunctions. Physica Status Solidi (A) Applications and Materials Science, 2008, 205, 2722-2728.	1.8	9
79	The effect of growth conditions on the properties of ZnO nanorod dye-sensitized solar cells. Materials Research Bulletin, 2008, 43, 3345-3351.	5.2	51
80	Snowflake-like ZnO structures: Self-assembled growth and characterization. Materials Letters, 2008, 62, 1761-1764.	2.6	17
81	Effect of Seed Layer on Structural Properties of ZnO Nanorod Arrays Grown by Vapor-Phase Transport. Journal of Physical Chemistry C, 2008, 112, 990-995.	3.1	96
82	Flame-synthesis of carbon nanotubes on silicon substrates and their field emission properties. Diamond and Related Materials, 2008, 17, 1015-1020.	3.9	7
83	Linear and nonlinear optical properties of ZnO nanorod arrays. Chinese Physics B, 2008, 17, 1291-1297.	1.4	16
84	Effect of adsorbates on field emission from flame-synthesized carbon nanotubes. Journal Physics D: Applied Physics, 2008, 41, 195401.	2.8	25
85	Fabrication and electrical, photosensitive properties of p-poly(9,9-diethylfluorene)/n-silicon nanowire heterojunction. Journal of Applied Physics, 2007, 102, .	2.5	18
86	Field emission from carbon nanotube bundle arrays grown on self-aligned ZnO nanorods. Nanotechnology, 2007, 18, 155702.	2.6	56
87	Structural, Photoluminescence, and Field Emission Properties of Vertically Well-Aligned ZnO Nanorod Arrays. Journal of Physical Chemistry C, 2007, 111, 12566-12571.	3.1	51
88	Influence of N2 flow ratio on the properties of hafnium nitride thin films prepared by DC magnetron sputtering. Applied Surface Science, 2007, 253, 8538-8542.	6.1	24
89	Field electron emission improvement of ZnO nanorod arrays after Ar plasma treatment. Applied Surface Science, 2007, 253, 8478-8482.	6.1	21
90	Multipod ZnO 3D microstructures. Materials Letters, 2007, 61, 3310-3313.	2.6	9

#	Article	IF	CITATIONS
91	Self-Organized ZnO Microcombs with Cuboid Nanobranches by Simple Thermal Evaporation. Crystal Growth and Design, 2006, 6, 2588-2591.	3.0	19
92	Synthesis and photoluminescence properties of vertically aligned ZnO nanorod–nanowall junction arrays on a ZnO-coated silicon substrate. Nanotechnology, 2006, 17, 3740-3744.	2.6	59
93	Silver Nanoisland Induced Synthesis of ZnO Nanostructures by Vapor Phase Transport. Journal of Nanoscience and Nanotechnology, 2006, 6, 1467-1473.	0.9	25
94	p-type transparent conducting oxides. Physica Status Solidi (A) Applications and Materials Science, 2006, 203, 1891-1900.	1.8	106
95	Fabrication and vacuum annealing of transparent conductive Ga-doped Zn0.9Mg0.10 thin films prepared by pulsed laser deposition technique. Applied Surface Science, 2006, 252, 8657-8661.	6.1	22
96	Water electrolysis-induced optical degradation of aluminum-doped zinc oxide films. Applied Surface Science, 2006, 253, 2547-2550.	6.1	1
97	Effect of substrate temperature on the growth and photoluminescence properties of vertically aligned ZnO nanostructures. Journal of Crystal Growth, 2006, 292, 19-25.	1.5	145
98	Controllable Synthesis of Vertically Aligned ZnO Nanorod Arrays in Aqueous Solution. Journal of Nanoscience and Nanotechnology, 2006, 6, 2062-2066.	0.9	14
99	Phase-segregation assisted growth of quasi-aligned ZnO nanorods on a Mg0.6Zn0.4O-coated Si substrate by thermal evaporation. Nanotechnology, 2006, 17, 5367-5372.	2.6	16
100	Oriented growth of p-type transparent conducting Ca-doped SrCu2O2 thin films by pulsed laser deposition. Semiconductor Science and Technology, 2006, 21, 586-590.	2.0	17
101	Raman spectroscopy and field electron emission properties of aligned silicon nanowire arrays. Physica E: Low-Dimensional Systems and Nanostructures, 2005, 30, 169-173.	2.7	47